IIETA International Information and Engineering Technology Association
Advancing the World of Information and Engineering

Annales de Chimie - Science des Matériaux
Vol. 50, No. 3, June, 2026, pp. 197-209
Journal homepage: http://iieta.org/journals/acsm

Performance and Microstructural Evaluation of Marine Algae-Derived Calcium Carbonate Filler for Partial Cement Replacement in Mortar

Remigildus Cornelis[1*], Papy Osias Alle[1], Debora Lau[1], Alvin Bara[2], Iwan Rustendi[3], Henricus Priyosulistyo[4]

[1] Department of Civil Engineering, Universitas Nusa Cendana, Kupang 85001, Indonesia
[2] Department of Building Engineering, Universitas Nusa Cendana, Kupang 85001, Indonesia
[3] Department of Civil Engineering, Universitas Wijaya Kusuma, Purwokerto 53152, Indonesia
[4] Department of Civil Engineering, Universitas Gadjah Mada, D.I. Yogyakarta 55281, Indonesia

Corresponding Author Email: remi@staf.undana.ac.id

https://doi.org/10.18280/acsm.500301

Received: 9 April 2026
Revised: 11 June 2026
Accepted: 20 June 2026
Available online: 30 June 2026

Keywords:
bio-based filler, calcium carbonate, cement replacement, marine algae, particle packing, mortar

ABSTRACT

Marine algae-derived calcium carbonate materials offer potential as sustainable fillers for reducing cement consumption in mortar. However, their effects on mortar performance and microstructure remain unclear. This study investigated the use of marine algae-derived bio-mineral filler (MAD-BMF), produced from Kappaphycus alvarezii, as a partial cement replacement at replacement levels of 5%, 10%, 15%, and 20%, with a constant water-to-binder ratio of 0.425. Fresh properties, setting time, compressive strength, and microstructural characteristics were evaluated through flow testing, setting-time measurements, X-ray fluorescence (XRF), X-ray diffraction (XRD), Fourier transform infrared (FTIR), and scanning electron microscopy-energy dispersive X-ray (SEM-EDX) analyses. Statistical analysis was performed using two-way ANOVA and Tukey's HSD test. Results showed that increasing MAD-BMF content reduced flowability and prolonged setting time due to the increased water demand associated with the fine particles. Compressive strength exhibited a non-linear response, with the highest value of 51.24 MPa at 28 days obtained at 10% replacement. Higher replacement levels reduced compressive strength because of the cement dilution effect. SEM observations indicated a denser matrix at moderate replacement levels, while XRD and FTIR analyses confirmed the absence of new hydration phases. XRF results showed that MAD-BMF was predominantly composed of calcium-based compounds, indicating its primary function as a $CaCO_3$-based filler. These findings demonstrate that MAD-BMF can replace up to 10% of Portland cement while maintaining or improving mortar performance through particle packing and matrix densification.

1. INTRODUCTION

Carbon emissions from the construction sector are a major global concern, largely driven by the intensive use of Portland cement. This is because cement production requires high energy input and releases significant CO_2, mainly from limestone decarbonation during clinker formation [1-3], serving as a major source of greenhouse gas emissions within the construction sector. However, the emissions are compounded by population growth and increased infrastructure development, which increases the scope and frequency of construction activity. This shows the need for developing material-based strategies to reduce the use of cement, while maintaining the engineering performance of mortar and concrete systems [4].

To limit the use of cement, non-reactive mineral filler can be partially substituted for cement in the production of concrete. The filler does not rely on chemical reactivity to improve the performance of concrete but functions through physical mechanisms, including the effect that increases particle packing density within the concrete matrix and refines microstructure [5]. In this context, marine algae have shown promising potential as bio-based partial cement replacement materials by functioning as non-reactive bio-mineral fillers in mortar systems. One promising species is Kappaphycus alvarezii, which contains a significant amount of calcium carbonate ($CaCO_3$) and has a distinctive morphology compared to other bio-mineral fillers [6-8].

When used as fine fillers in low to moderate amounts, bio-based materials enhance the structural compactness of mortar by refining the pore structure and promoting a more uniform particle distribution, leading to a robust hardened-state product. However, excessive replacement reduces the amount of reactive cement available for hydration, resulting in lower strength. Therefore, determining the optimum level of fine filler replacement is very important. Since particle attributes significantly impact early-age behavior and the workability of mortar, both fresh-state properties and microstructure should be assessed alongside the mechanical performance of the mortar [9].

The extensive cultivation of Kappaphycus alvarezii in tropical regions, with Indonesia being one of the largest producers globally, has ensured a substantial and reliable supply of biomass [10, 11]. This abundance creates opportunities for value-added products through the generation of marine algae-derived bio-mineral filler (MAD-BMF), while reducing dependence on conventional cementitious materials. Furthermore, this abundant biomass enables marine algae to transition from primary commodity to a functional raw material used in construction material systems, as well as support the principles of resource efficiency and the bioeconomy in developing new materials.

Previous studies on algae-based cementitious materials have primarily evaluated compressive strength, workability, and hydration behavior, with several reporting improvements in engineering performance following the incorporation of algae-derived powders [12, 13]. However, the mechanisms by which particle packing, matrix densification, and cement dilution influence mortar performance across different replacement levels remain insufficiently understood. In addition, studies specifically investigating marine algae-derived calcium carbonate as a bio-based inert filler are still limited, particularly those integrating mechanical testing with statistical and complementary microstructural characterization to explain its role in mortar performance.

To address these gaps, this study integrates mechanical testing with statistical and complementary microstructural analyses to investigate how particle packing, matrix densification, and cement dilution contribute to mortar performance across different replacement levels and to identify the optimum substitution level of marine algae-derived $CaCO_3$ bio-mineral filler.

Accordingly, this study investigates the influence of MAD-BMF on the fresh properties, compressive strength, and microstructural characteristics of mortar to determine the optimum substitution level and clarify the physical mechanisms governing mortar performance.

2. MATERIALS, METHODS AND EXPERIMENTAL PROCEDURE

All experimental activities were conducted in the laboratories of the Department of Civil Engineering at Nusa Cendana University, Kupang, Indonesia. Laboratory testing was performed under ambient conditions, at relative humidity levels of 80% to 95%, and temperatures ranging from 20 ℃ to 37 ℃. Although ambient environmental conditions were not strictly controlled, all mixtures were prepared, cured, and tested following the same procedures within the same laboratory, ensuring consistent experimental conditions for all specimens. Therefore, environmental variation is acknowledged as a limitation that may influence early-age behavior, but it is unlikely to affect the comparative evaluation among mixtures.

Subsequently, the hardened specimens were cured in a water curing tank at 23 ± 2 ℃ (ASTM standard). The experimental program consisted of four main phases, including preparation of raw material and processing of marine algae powder, determining the proportions for the mortar mix, casting and curing the mortar, and performing the mechanical and microstructural testing. The materials used to produce the mortar included Portland cement, locally available sand from a river, and marine algae powder. The algae were prepared and processed in the bioscience laboratory, while all mortar production and testing operations were conducted in the Civil Engineering laboratory at Nusa Cendana University.

2.1 Raw materials

2.1.1 Algae

Marine algae collected from coastal regions were washed with fresh water to remove adhering salts and surface impurities. The algae were initially sun-dried to reduce their moisture content and subsequently oven-dried at 100 ℃ for 24 h to remove residual moisture. After cooling to room temperature, the dried algae were ground into a fine powder using a laboratory grinder and passed through a 75 μm (200-mesh) sieve to obtain a uniform maximum particle size. The resulting powder had a specific gravity of 2.8. Because particle size distribution (PSD) and specific surface area (SSA) measurements were unavailable, the discussion regarding particle-size effects is based on the nominal maximum particle size (75 μm) and observed microstructural behavior. Future studies should quantify PSD and SSA to improve reproducibility.

2.1.2 Portland cement

The only binding agent used in all mortar mixes was Portland cement (PPC) obtained from a local supplier in Kupang, Indonesia. There was no treatment provided, and the specific gravity of the binder was found to be 3.15 when measured according to the procedures outlined in ASTM C188 [14].

2.1.3 Fine aggregate

In all mortar mixes, natural river sand obtained locally was used as the fine aggregate. The fine aggregate for mortar was evaluated to determine several characteristics, including bulk density, water absorption, and specific gravity.

Table 1. Physical properties of natural river sand

Material	Specific Gravity (SSD)	Absorption (%)	Fineness Modulus
Fine Aggregate	2.64	2.14	3.065

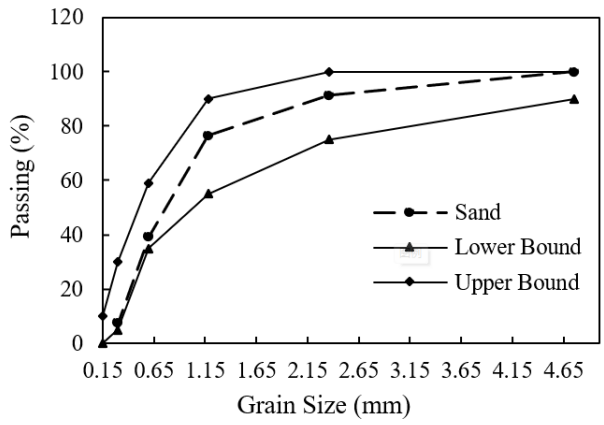

Figure 1. Sieve analysis of sand

The methods used for performing these characterizations adhered to ASTM C128-22 [15]. PSD was determined by sieve analysis in accordance with ASTM C136/C136M-19 [16] and ASTM C33/C33M-18 [17], and the fineness modulus

of the sand translated to coarse grading, with an actual unit weight of 1638.12 kg/m³. A summary of the physical characteristics of the sand is shown in Table 1, and a grading curve is presented in Figure 1.

2.2 Method and mix procedures

2.2.1 Specimen preparation and curing

The mix proportion was determined using the absolute volume method, which allowed the precise control of the volumetric contribution of each constituent material within the mortar mix. In this method, the compactness of the mortar was defined by assuming that one cubic metre of mortar was occupied by the sum of all absolute volumes of the four constituent materials, including cement (V_c), the fine aggregate (V_s), mixing water (V_w), and MAD-BMF (V_a). Using this relationship, the following volumetric relationship was adopted, as set out in Eq. (1) [18-20]:

$$V_c + V_s + V_w + V_{al} = 1\text{m}^3 \quad (1)$$

The volume of voids within the sand was calculated by considering a condition where pore spaces were fully occupied by cement paste. This calculation was performed using the apparent specific gravity of the sand (Gs_s) combined with the saturated surface-dry unit weight (W_s).

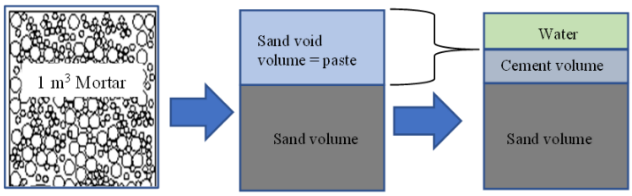

Figure 2. The absolute volume concept of mortar mix

Figure 2 schematically illustrates the absolute volume method adopted for the mortar mix design.

The calculated sand void volume (Vv_s) was determined using Eq. (2) as follows:

$$Vv_s = 1 - \frac{W_s}{Gs_s\gamma_w} \quad (2)$$

where, γ_w is the unit weight of water, assumed to be 1000 kg/m³, W_s is the mass of sand, and Gs_s is the specific gravity of sand. The calculated sand void volume was used to determine the minimum paste volume required to fill the pore spaces between sand particles. Based on the measured bulk density and specific gravity of the sand, the calculated paste-to-void ratio (R) for the reference mixture was approximately 1.0. This value resulted directly from the measured aggregate properties and the adopted absolute-volume mix design rather than from an arbitrary assumption. This procedure follows the aggregate packing concept, in which the required paste volume is determined from the measured void volume of the aggregate skeleton [21]. The paste-to-void ratio has also been used as a governing mix design parameter for geopolymer mortar and concrete [19, 22]. In those studies, an optimum R value of 1.5 was identified experimentally for the specific geopolymer systems investigated and was subsequently adopted in geopolymer concrete mixture design. Because the present study employed ordinary Portland cement as the primary binder rather than an alkali-activated geopolymer binder, that optimized R value was not directly applicable to the present system. Instead, the calculated paste-to-void ratio was maintained constant while only the MAD-BMF replacement level was varied throughout the experimental program.

The mix design relationship based on the absolute volume method is provided in Eq. (3).

$$\frac{W_c}{Gs_c\gamma_w} + \frac{W_s}{Gs_s\gamma_w} + \frac{W_w}{Gs_w\gamma_w} + \frac{W_{al}}{Gs_{al}\cdot\gamma_w} = 1 \quad (3)$$

where, the weight of cement is W_c, the specific gravity of cement is Gs_c, the weight of water is W_w, the specific gravity of water is Gs_w of 1, the weight of MAD-BMF is W_{al}, and the specific gravity of MAD-BMF is Gs_{al}. Eq. (4) is obtained by simplifying Eq. (3) under the assumptions of a cement-to-sand mass ratio of 1: p, where p is the sand-to-cement ratio, R_{wc} is the water-to-cement ratio, and S_{al} is the mass replacement ratio of MAD-BMF.

$$\frac{W_c(1-S_{al})}{Gs_c\gamma_w} + \frac{PW_c}{Gs_s\gamma_w} + \frac{R_{wc}W_c}{Gs_w\gamma_w} + \frac{S_{al}W_c}{Gs_{al}\gamma_w} = 1 \quad (4)$$

This equation yields per cubic meter, as shown in Eq. (5):

$$W_c = \frac{\gamma_w}{\left[\frac{(1-S_{al})}{Gs_c} + \frac{p}{Gs_s} + \frac{R_{wc}}{Gs_w} + \frac{S_{al}}{Gs_{al}}\right]} \quad (5)$$

Eq. (5) was used to establish the reference mortar mixture. For the experimental program, the reference mixture was maintained while cement was partially replaced by MAD-BMF on a mass basis. The sand and water contents were kept constant to isolate the effect of MAD-BMF replacement. The resulting mix proportions are presented in Table 2.

The absolute-volume method was used only to establish the reference mixture, whereas the subsequent experimental mixtures were prepared by replacing cement with MAD-BMF on a constant mass basis while maintaining constant sand and water contents.

Table 2. Composition of mortar with and without marine algae-derived bio-mineral filler (MAD-BMF) as bio-mineral filler

ID Sample	Marine Algal Powder [W_{al}] (%)	(Kg)	Cement [W_c] (kg)	Sand [W_s] (kg)	Water [W_w] (kg)
MN	0.0	0.00	887.25	887.25	377.08
MA5	5	39.43	842.9	883.75	375.59
MA10	10	78.87	798.53	883.75	375.59
MA15	15	118.3	754.16	883.75	375.59
MA20	20	157.73	709.8	883.75	375.59

Table 3 shows the paste mixes prepared independently for setting-time tests, which do not follow the absolute-volume design applied to the mortar mixes.

The reference composition was adopted as the baseline to evaluate the influence of marine algae powder while maintaining all other mix parameters unchanged. A set of preliminary mortar mixes was prepared by systematically adjusting the water-to-cement ratio within the range of 0.325 to 0.625 at intervals of 0.05, in combination with cement-to-sand ratios of 1:1, 1:2, and 1:3. The selection of the reference mix (MN) was based on an integrated assessment of fresh-state workability and 28-day compressive strength, leading to a mix

with a water-to-cement ratio of 0.425 and a sand-to-cement ratio of 1.

For the base mix of MN, the maximum replacement level of cement with marine algae powders should be 20% by mass with increments of 5% throughout the experimental program. Therefore, the samples for the measurement of the time for the setting of the paste were designated as C0 (0%), CAL5 (5%), CAL10 (10%), CAL15 (15%), and CAL20 (20%), as presented in Table 3. For mortar used in flow and compressive strength tests, the samples were labelled MN, MA5, MA10, MA15, and MA20 (Table 2). Substituting a maximum of 20% was based on a review of previously published literature, showing the possibility of reduced workability and interference with cement hydration at levels greater than 20%. Furthermore, the experimental design was established by holding constant the amounts of sand and water, while increasing MAD-BMF.

Table 3. Composition of paste with and without marine algae-derived bio-mineral filler (MAD-BMF) as bio-mineral filler

No.	ID Sample	Marine Algal Powder [W_{al}] (%)	(Kg)	Cement [W_c] (kg)	Sand [W_s] (kg)	Water [W_w] (kg)
1	C0	0	0	0.300	-	0.075
2	CAL5	5	0.015	0.235	-	0.075
3	CAL10	10	0.03	0.220	-	0.075
4	CAL15	15	0.045	0.205	-	0.075
5	CAL20	20	0.06	0.190	-	0.075

2.2.2 Data analysis

A completely randomized design (CRD) was adopted for this laboratory study, which was considered suitable for experiments conducted under controlled conditions using homogeneous experimental units. All specimens were prepared using identical raw materials, mixing procedures, curing conditions, and testing methods to minimize the influence of uncontrolled variables.

The experiment followed a factorial design with two factors, namely MAD-BMF content (five levels) and curing age (three levels), comprising three replicates for each combination. A two-way ANOVA was applied to evaluate the effects of these factors on compressive strength, followed by Tukey's HSD test for pairwise comparisons.

Before ANOVA, the assumptions of normality and homogeneity of variance were assessed using the Shapiro–Wilk and Levene's tests, respectively. When significant differences were detected ($p < 0.05$), post-hoc comparisons were conducted to identify specific group differences. All statistical analyses were performed using SPSS.

2.2.3 Microstructure characterization

The performance of MAD-BMF was evaluated alongside the reference mortar through examinations of both fresh and hardened states. Fresh-state properties were evaluated by measuring the setting time and flowability, while hardened properties were assessed through compressive strength testing. Additional microstructural and chemical analyses were used to provide insights regarding the role of marine algal powder in cementing systems through scanning electron microscopy-energy dispersive X-ray (SEM-EDX) analysis, X-ray diffraction (XRD), X-ray fluorescence (XRF), and Fourier transform infrared (FTIR) analysis.

Using the Vicat apparatus, ASTM C191-21 [23] was used to evaluate the determination of cement paste setting time, and the workability of fresh mortar was evaluated using the flow table method in conjunction with ASTM C1437-20 [24]. For compressive strength testing, cube specimens with dimensions of 50 × 50 × 50 mm³ were tested after demolding at 24 hours, followed by curing in water. Compressive strength tests were conducted at 7, 14, and 28 days in accordance with ASTM C109/C109M-20 [25]. A total of three replicate specimens (n = 3) were tested for each mix and curing age. The reported values represented the mean compressive strength, and the standard deviation was calculated to quantify the variability of the results. The phases contained in the material were identified by XRD (Bruker AXS D8 Advance Eco), elemental analysis was performed using an XRF spectrometer (Rigaku NEX QC+ QuantEZ, 2015), microstructural features were characterized using SEM-EDX analysis (JEOL JSM-6510LA), and functional groups were determined with FTIR spectroscopy (Thermo Scientific Nicolet iS10). The overall experimental program was designed as an exploratory and performance-based study of the feasibility of using marine algae powders as a bio-mineral filler material in mortar applications.

3. EXPERIMENTAL RESULTS

This section presents experimental results related to the macroscopic and microscopic characteristics of MAD-BMF mortar. The macroscopic characteristics observed included setting behavior, workability, and compressive strength development, while the microscopic characteristics comprised the mortar's microstructural configuration.

3.1 Fresh properties and early-age behavior

Figure 3 shows the penetration characteristics, showing the presence of a retardation effect in cement paste incorporating MAD-BMF compared with the control cement paste. Each setting time value represents the average of three independent measurements (n = 3). The experimental data showed that partial substitution of Portland cement with MAD-BMF contributed to the retardation of initial setting. For example, the control paste reached its initial setting time at approximately 103 minutes, while all pastes containing MAD-BMF required a longer time to attain both initial and final setting times. Similarly, Boukhatem et al. [26, 27] reported that the hydration process in cement systems incorporating MAD-BMF was delayed.

Figure 4 shows the non-linear relationship between MAD-BMF content and the setting time of cement paste. At a substitution level of 5%, the initial and final setting times were recorded as 136.93 minutes and 235 minutes, respectively, which were longer than those of the control paste. At a 10% substitution level, the initial and final setting times decreased to 121.06 minutes and 225 minutes, respectively, compared with the 5% mix, but remained longer than those of the control

paste. When the MAD-BMF substitution level reached 15% or higher, a renewed retardation of both initial and final setting times was observed.

Based on these results, the obtained data did not show a clear concentration–effect relationship between the MAD-BMF substitution level and the setting time of cement paste. However, the results confirmed that using MAD-BMF as a cement substitute significantly influenced the early-age initial setting behavior of cement paste. The effects on rheological properties and cement hydration during the early hydration period will be discussed in the discussion section of this study.

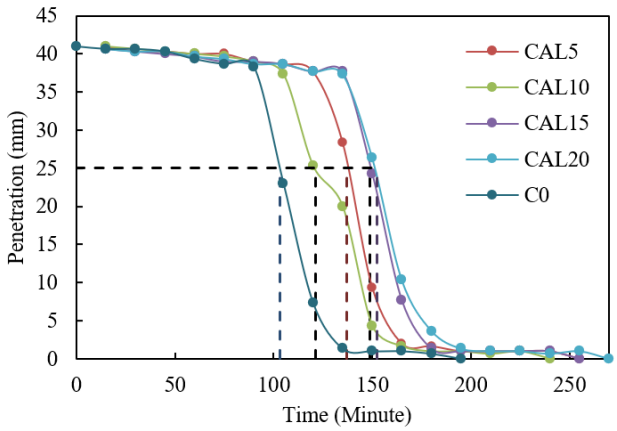

Figure 3. Setting time of paste with and without marine algae-derived bio-mineral filler (MAD-BMF)

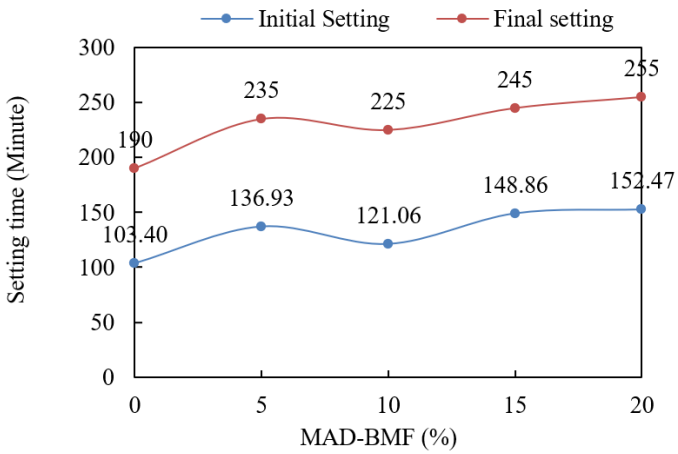

Figure 4. Effect of marine algae-derived bio-mineral filler (MAD-BMF) substitution on setting time

Figure 5 presents the effect of MAD-BMF on the flow characteristics of mortar, with the MN showing a flow value of 111%. Partial substitution of cement with MAD-BMF caused a gradual reduction in mortar flow as the substitution level increased. Based on the graphical results, flow values of 110.45%, 110.05%, and 109.11% were obtained at substitution levels of 5%, 10%, and 15%, respectively. The mix containing 20% MAD-BMF showed the lowest flow value, at 108.36%.

The results were consistent with the reports by Boukhatem et al. [26], who observed that the viscosity of the mix increased with rising levels of MAD-BMF substitution. The increase in viscosity led to higher resistance to flow, causing the mortar to become more viscous and a reduction in flow value.

In line with the analysis, a gradual decrease in workability was observed with increasing MAD-BMF content. However, all measured flow values remained within the acceptable range specified by ASTM C1437 [24]. These results showed that the level of MAD-BMF substitution consistently affected the workability of the mortar, providing a basis for further discussion of the rheological behavior.

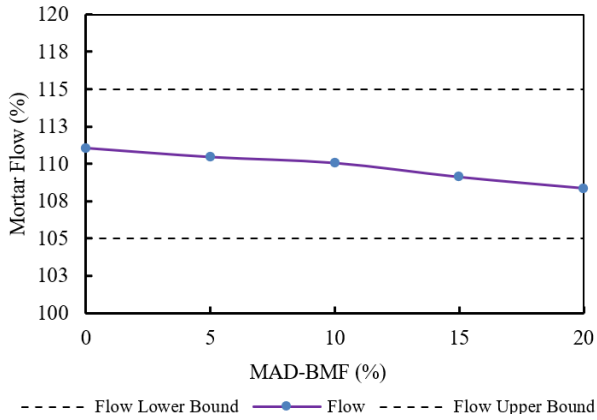

Figure 5. Effect of cement substitution with marine algae-derived bio-mineral filler (MAD-BMF) on mortar flow

3.2 Compressive strength results

Table 4 shows that compressive strength increases with curing age for all mixes. The incorporation of MAD-BMF enhanced compressive strength, reaching an optimum at 10% substitution, with a significant improvement compared to the control mortar at all testing ages. However, at higher replacement levels (≥15%), compressive strength decreased due to the dominance of the dilution effect. The relatively low standard deviation values showed good consistency and reliability of the test results.

Table 4. Compressive strength of mortar incorporating marine algae-derived bio-mineral filler (MAD-BMF) at different curing ages

MAD-BMF Content (%)	7 Days (MPa)	14 Days (MPa)	28 Days (MPa)
0	25.24 ± 1.55	35.69 ± 2.43	40.50 ± 2.19
5	35.11 ± 2.72	43.21 ± 1.38	48.86 ± 1.80
10	37.72 ± 2.47	46.16 ± 1.62	51.24 ± 1.64
15	33.05 ± 2.54	40.88 ± 0.87	42.37 ± 2.62
20	29.76 ± 1.20	37.50 ± 2.40	39.46 ± 1.05

Figure 6 shows distinct differences in mechanical behavior during compressive strength testing between the MN and the MA10. In the MN specimens, failure was dominated by the rapid formation of major vertical cracks, leading to partial spalling at the core and edge regions of the specimens. The MA10 specimens showed a more gradual crack development, with a more uniform distribution of both vertical and inclined cracks before ultimate failure. Additionally, no early-stage spalling was observed in the MA10 specimens, and crack-related damage was more uniformly distributed along the height of the specimens compared with MN. This observation indicates that the modified mortar matrix became more homogeneous and dense, thereby altering the macroscopic

failure pattern during the fracture process and causing a more gradual and controlled failure mechanism in MA10 compared with MN.

(a)

(b)

Figure 6. Crack pattern (a) MN, and (b) MA10

As presented in Figure 7, the control mix showed an increase in compressive strength from approximately 25 MPa at 7 days to 40 MPa at 28 days, with a corresponding flow value of 112%. Partial substitution of cement with MAD-BMF caused a rise in compressive strength at all curing ages. The MA10 specimens showed the most significant improvement, increasing from 38 MPa at 7 days to 51 MPa at 28 days. However, at substitution levels exceeding 10%, a reversal trend was observed, showing a reduction in compressive strength performance at higher contents. These results showed that compressive strength did not increase linearly with rising MAD-BMF content in the mix. When correlated with the flow properties shown in Figure 8, the flow values at MAD-BMF substitution levels of approximately 10% remained within the acceptable range specified by ASTM C1437 [24], although a decreasing trend in flow was observed with increasing content.

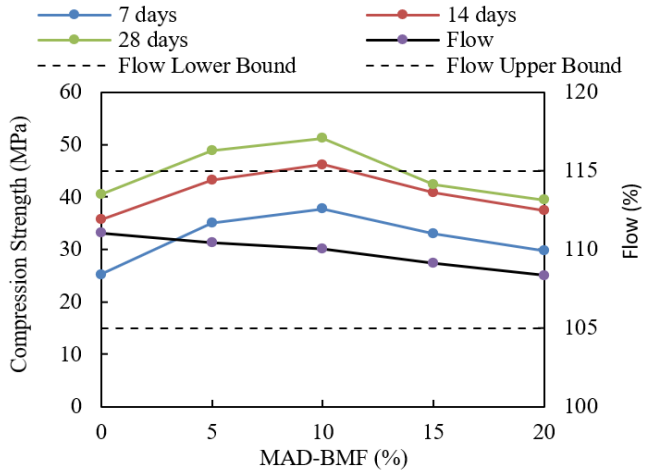

Figure 7. Effect of cement substitution with marine algae-derived bio-mineral filler (MAD-BMF) on the compressive strength and flow of mortar.

3.3 Statistical analysis

The assumptions of normality and homogeneity of variance were satisfied ($p > 0.05$). The two-way ANOVA results showed that curing age and MAD-BMF content significantly affected compressive strength ($p < 0.001$). The interaction between curing age and MAD-BMF content was not statistically significant ($p = 0.208$), indicating that the effect of MAD-BMF remained consistent across different curing ages (Table 5).

Tukey's post-hoc analysis showed that the 10% substitution level had the highest compressive strength and differed significantly from the 0% and 20% levels ($p < 0.05$), but not from the 5% and 15% levels (Table 6). For curing age, compressive strength at 7 days was significantly lower than at 14 and 28 days, without showing substantial differences (Table 7).

Table 5. Results of two-way ANOVA for compressive strength

Source of Variation	df	SS	MS	F-Value	p-Value
Curing age	2	1191.49	595.75	147.5	<0.001
MAD-BMF content	4	779.81	194.95	48.27	<0.001
Interaction	8	47.62	5.95	1.47	0.208
Error	30	121.17	4.04	—	—
Total	44	2140.09	—	—	—

Table 6. Tukey's HSD post-hoc test results for marine algae-derived bio-mineral filler (MAD-BMF) content

MAD-BMF Content (%)	Compressive Strength (MPa)	Group
10	51.24	a
5	48.86	ab
15	42.37	bc
0	40.50	c
20	39.46	c

Notes: Different letters show statistically significant differences ($p < 0.05$).

Table 7. Tukey's HSD post-hoc test results for curing age

Curing Age (days)	Compressive Strength (MPa)	Group
28	44.49	a
14	40.69	a
7	32.18	b

Notes: Different letters show statistically significant differences ($p < 0.05$).

3.4 Microstructural characteristics

3.4.1 Characterization X-ray fluorescence

As presented in Table 8, XRF results showed changes in oxide composition after incorporating 10% MAD-BMF (MA10). The MN was dominated by SiO_2 (29.15%) and CaO (27.94%), representing typical contributions from sand and cement. In MA10, CaO increased to 31.7%, confirming the presence of calcium-rich phases derived from the algae, while SiO_2 slightly decreased to 28.01% due to dilution of the siliceous fraction.

Minor reductions in Al_2O_3 and Fe_2O_3 further supported this dilution effect, showing that MAD-BMF did not introduce significant reactive aluminosilicate phases. The low SO_3 content in both mixes suggested minimal influence on sulfate-related compounds. Meanwhile, slight increases in Na_2O and K_2O were attributed to the marine origin of the algae.

Table 8. Results of the X-ray fluorescence (XRF) analysis

Oxide	CaO	SiO_2	SO_3	Al_2O_3	Fe_2O_3	MgO	K_2O	Na_2O
MN	27.94	29.15	0.776	6.02	2.251	2.3	0.6	0.25
MA10	31.7	28.01	0.15	5.69	2.207	2.1	0.8	0.65

The incomplete oxide total was attributed to loss on ignition (LOI), linked to carbonate decomposition. Overall, the results confirmed that MAD-BMF acted as a $CaCO_3$-based, non-reactive filler, modifying the system primarily through calcium enrichment and dilution effects.

3.4.2 Scanning electron microscopy-energy dispersive X-ray analysis

SEM observations of the MAD-BMF in Figures 8 and 9 revealed that the material consisted of relatively small particles of irregular shape and roughened surface areas with a high degree of porosity.

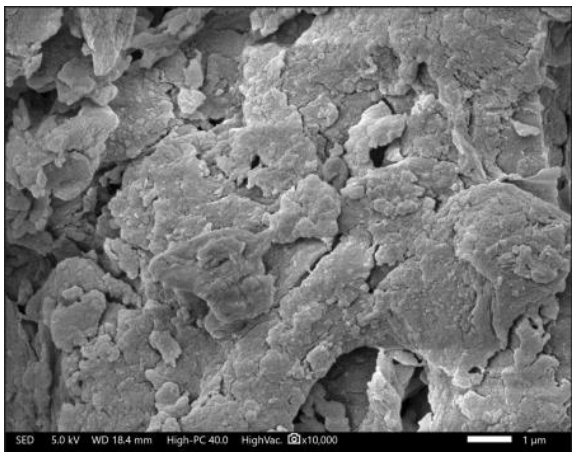

(a)

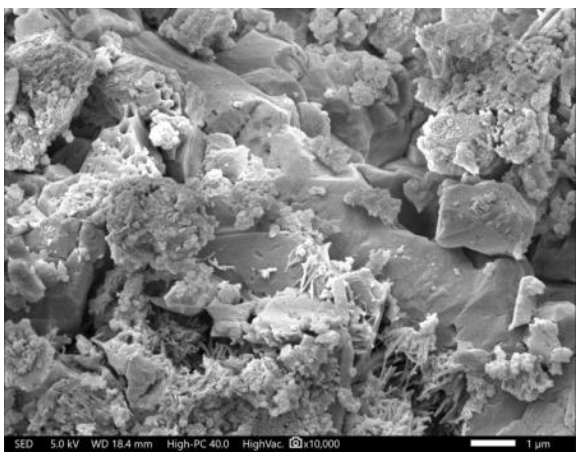

(b)

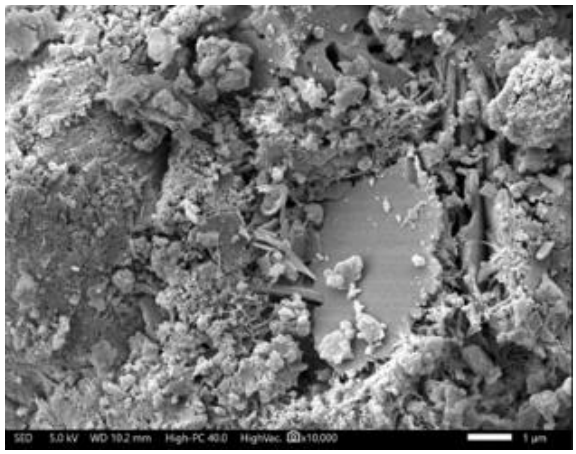

(c)

Figure 8. Scanning electron microscopy (SEM) micrographs of (a) MAD-BMF, (b) MN, and (c) MA10

The corresponding EDX analysis showed that MAD-BMF consisted predominantly of calcium and oxygen, with only trace amounts of other elements. This composition confirmed that the material's enhanced performance was largely attributable to the high content of calcium-based minerals.

The SEM images of the MN showed the cement matrix, whereby hydration products were spread uniformly, but micro-scale voids and pores were present between particles. The elemental analysis completed at locations SPC-001 to SPC-004 indicated that the chemical composition was largely comprised of Ca, Si, and O, which corresponded with the principal hydration phases in Portland cement type systems.

In comparison, the MA10 showed a more compact matrix structure, characterized by a substantial reduction in internal pore space. There were also MAD-BMF particles embedded and dispersed randomly throughout the cement paste. The EDX data taken from SPC-005 through SPC-008 showed Ca-Si-O type spectra with a more uniform distribution of elements compared to the equivalent locations of MN, without the presence of any other phases.

3.4.3 Characterization Fourier transform infrared

The FTIR spectra presented in Figure 10 showed that the MN, MA10, and MA20 shared comparable characteristic absorption features.

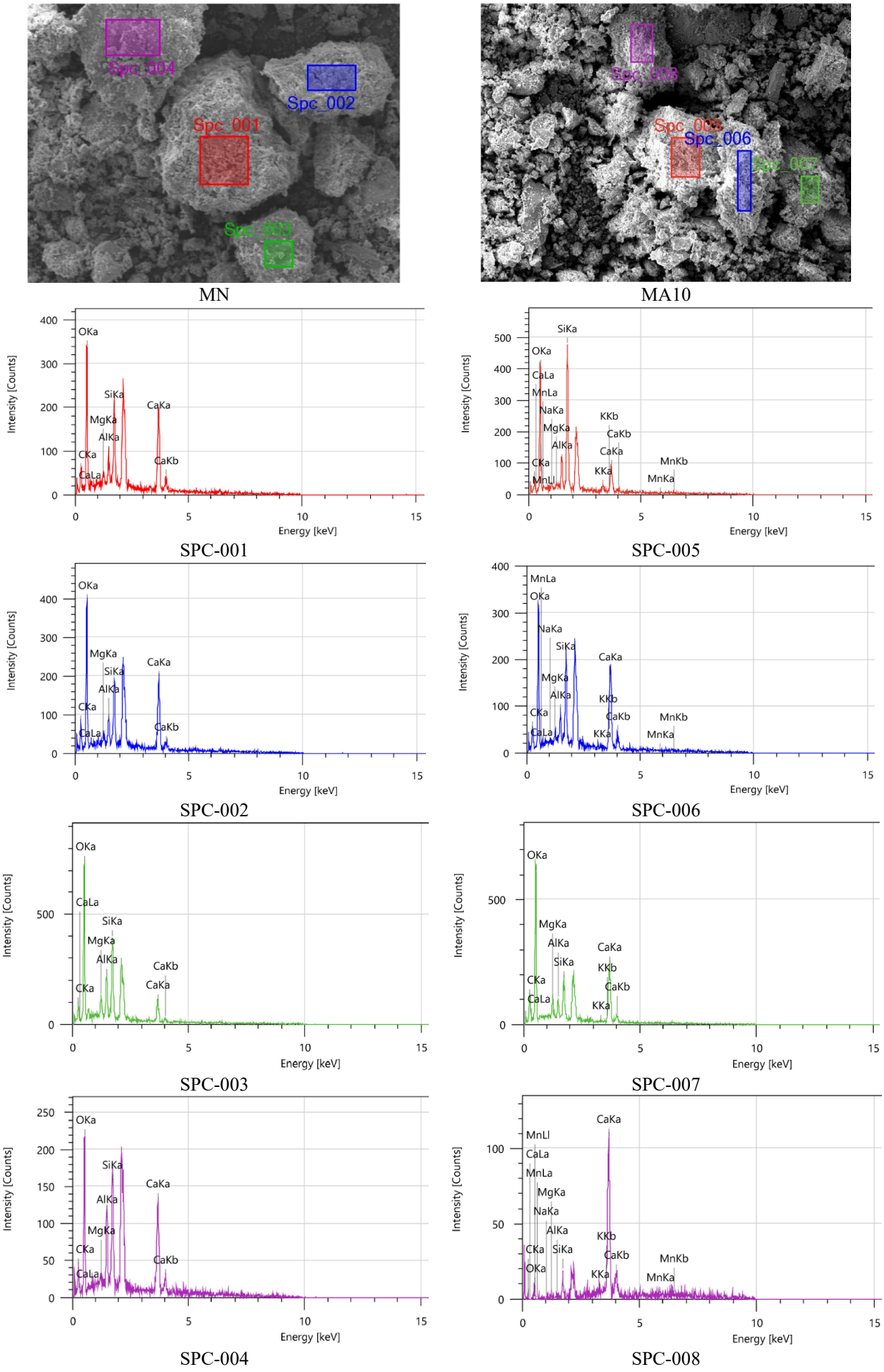

Figure 9. Energy dispersive X-ray (EDX) analysis of MN and MA10

Across all mixes, a broad absorption band appearing in the region of approximately 3400-3500 cm^{-1}, together with a distinct band near 1640 cm^{-1}, could be observed. These features were attributed to the stretching and bending vibrations associated with hydroxyl (–OH) groups present in the cementitious matrix.

All mixes exhibited similar spectral characteristics in the wavenumber range of approximately 1400 to 1450 cm^{-1}, which corresponded to the asymmetric vibrational modes of carbonate (CO_3^{2-}) groups. Spectral bands in the approximately 950-1000 cm^{-1} range were also present, which were attributed to stretching vibrations associated with silica as part of the silica glass structure. The addition of MAD-BMF did not produce any new bands or significant shifts (greater than 1 cm), relative to MN. This showed that the basic chemical nature of the cement was unchanged despite the addition of MAD-BMF.

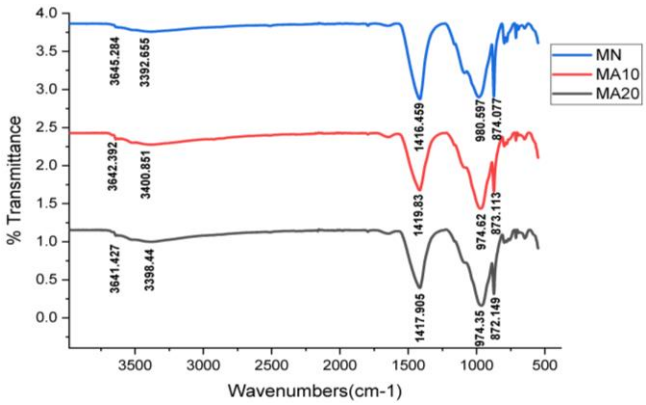

Figure 10. Fourier transform infrared (FTIR) spectra of MN, MA10, and MA20

3.4.4 characterization X-ray diffraction

Crystal structure analysis using XRD on MAD-BMF specimens (Figure 11) showed that the material consisted of predominantly crystalline forms of $CaCO_3$ in the form of calcite, the dominant phase. The comparison of XRD pattern results for MN and MA10 indicated that both actually provided similar XRD patterns, showing their respective polymorphs have the same crystalline compounds, portlandite and calcite. When incorporating MAD-BMF into MN, no other crystallographic phases were created.

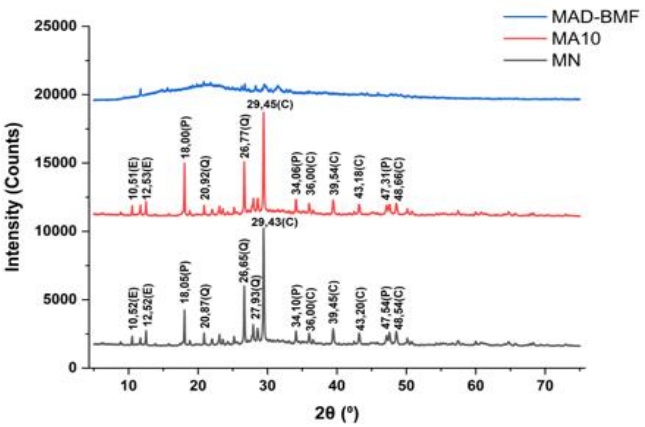

Figure 11. X-ray diffraction (XRD) patterns of MAD-BMF, control mortar (MN), and mortar containing 10% MAD-BMF (MA10)

Note: Diffraction patterns were vertically offset for clarity.

Consistent with the XRD results, the FTIR analysis confirmed the presence of similar functional groups across all samples. The characteristic bands corresponding to –OH stretching, CO_3^{2-}, and Si–O groups were observed in each specimen, further showing that the incorporation of MAD-BMF did not introduce new functional groups into the otherwise inert matrix.

The different results from microstructural characteristics, phase characterization, spectroscopic methods, and chemical analysis served as determinants of differences between MN and MAD-BMF modified. These differences would be considered further in the engineering properties in the discussion section.

4. DISCUSSION

4.1 Particle interactions and fresh-state behavior

The fresh-state behavior of the mortar is governed by changes in interparticle interactions and water distribution induced by MAD-BMF incorporation, establishing the initial conditions that control hydration and strength development. As the substitution level increases, flowability decreases, showing that particle-scale effects dominate system behavior. This reduction arises from the higher SSA of fine particles, which increases water demand and shifts the balance between solid particles and available mixing water.

To maintain particle stability, the system requires additional water, resulting in higher water demand. Consequently, less free water remains available for flow. This condition intensifies interparticle contact and increases resistance to movement, showing the role of interparticle forces and particle packing in controlling rheological behavior as reported by Yuan et al. [28].

The same mechanism governs setting behavior by constraining the availability of free water required for early hydration. Reduced free water limits ion mobility and slows the progression of hydration reactions, leading to delayed setting times. Similar behavior has been reported in systems incorporating fine $CaCO_3$ particles, where increased water demand and modified PSD influence hydration kinetics [29, 30].

In line with the analysis, fresh-state properties are governed by physical interactions at the particle-scale, defined by the relationship between surface area, available water, and interparticle contact. These conditions constrain hydration kinetics and other strength development by limiting effective water availability and modifying particle packing efficiency.

4.2 Chemical composition and reactivity of marine algae-derived bio-mineral filler

The chemical composition defines the reactivity boundary of the system, confirming that MAD-BMF does not contribute to chemical reactions and isolating the role of physical mechanisms in controlling performance. The XRF results show an increase in CaO content accompanied by a reduction in SiO_2 and Al_2O_3. This indicates a shift toward a calcium-dominated composition. This compositional change excludes pozzolanic behavior, as the absence of reactive aluminosilicate phases prevents secondary hydration reactions.

The interpretation is consistent with $CaCO_3$-based filler systems, where materials primarily influence performance

through physical effects without significantly altering hydration chemistry, as reported by Scrivener et al. [31]. In comparison, reactive supplementary materials such as fly ash enhance strength through pozzolanic reactions driven by higher reactive silica content.

A previous study by Acarturk et al. [32] stated that bio-based materials could introduce alkali components. However, this study showed that Na_2O and K_2O remained at low levels and did not affect system reactivity. The unaccounted oxide fraction corresponded to LOI, confirming the presence of carbonate phases associated with $CaCO_3$ decomposition.

The results collectively show that MAD-BMF functions as a $CaCO_3$-based inert filler, where system behavior is governed by compositional characteristics, facilitating physical interactions over chemical reactivity.

4.3 Particle packing and dilution mechanisms in strength development

The balance between particle packing and cement dilution influences strength development, with an optimum level showing a transition between packing-dominated and dilution-controlled behavior. Compressive strength shows a non-linear relationship, with an optimum at 10%, indicating the balance between particle packing and cement dilution. At low replacement levels, fine MAD-BMF particles fill voids, reduce porosity, and improve load transfer, leading to strength enhancement. This mechanism is consistent with particle packing theory, where improved packing density enhances mechanical performance.

At higher replacement levels, reduced cement content limits hydration product formation, leading to strength reduction. Previous studies by Lothenbach et al. [33] on limestone filler reported an optimum substitution range of approximately 10–15%, showing a higher sensitivity to cement dilution. Berodier and Scrivener [34] reported that irregular particle morphology could reduce packing efficiency at higher replacement levels, confirming the observed decline in strength beyond 10% replacement. Therefore, strength development is controlled by densification effects under limited binder availability. Above 10%, cement content decreases, hydration products reduce, and the matrix weakens. Strength decreases significantly, confirming that performance is governed by the balance between packing efficiency and cement dilution rather than chemical reactivity.

4.4 Statistical evaluation of strength development and optimum threshold

Statistical analysis confirms the significance of the observed performance trends and validates the existence of a distinct optimum threshold associated with the governing mechanism. The results of two-way ANOVA showed that MAD-BMF content and curing age significantly affected compressive strength, while their interaction was not substantial. This shows that the effect of MAD-BMF is consistent across curing ages.

Tukey analysis shows that the 10% substitution level has the highest compressive strength and differs significantly from the lowest levels (0% and 20%), but not from intermediate levels (5% and 15%). This pattern shows an optimum trend rather than complete statistical separation across all levels.

The results are consistent with the concept of packing-controlled systems, where performance is governed by structural arrangement rather than chemical evolution [35, 36]. In comparison, reactive systems typically show time-dependent interactions due to hydration kinetics [32]. The absence of interaction effects in this study shows that the governing mechanism remains stable over time.

4.5 Microstructural evidence of matrix densification

Microstructural observations provide direct evidence supporting the proposed mechanism by showing the effect of particle packing on matrix densification. SEM observations show a denser matrix at 10% substitution, characterized by reduced pore space and improved particle distribution. This shows that strength enhancement is governed by packing-induced densification rather than chemical effects. However, XRD and FTIR analyses show no formation of new hydration phases, confirming the absence of chemical contribution.

XRF defines the chemical composition, and SEM characterizes the microstructure. Mechanical results provide direct evidence of performance. The consistency among these results supports a unified mechanism, where matrix densification governs strength development. Similarly, Scrivener et al. [31] and Fathy et al. [37] reported that mechanical performance in $CaCO_3$-based filler systems was primarily governed by pore refinement and particle packing rather than hydration reactions [31, 37].

The results show that the role of MAD-BMF is primarily physical, operating through particle packing and microstructural refinement. The relationship between compositional, microstructural, and mechanical results confirms that the observed strength enhancement originates from improved matrix compactness rather than additional hydration products.

4.6 Design implications for cement reduction using bio-based filler

The identified mechanism provides a basis for designing cementitious systems, where performance can be optimized through controlled particle packing and substitution levels. MAD-BMF behaves similarly to limestone filler but originates from marine biomass, functioning as a bio-based $CaCO_3$ inert filler. Reactive materials such as fly ash and slag depend on chemical reactions and hydration kinetics, as shown by Berodier et al. [34] and Juenger et al. [38], which introduces variability.

MAD-BMF follows a different pathway, depending on particle packing. The observed response is predictable and primarily influenced by particle distribution and dosage, rather than reaction kinetics. Therefore, this study transitions from chemical reactivity to controlled physical mechanisms in sustainable cementitious materials.

4.7 Mechanistic insights into cement substitution in bio-based filler systems

To contextualize the proposed design method, the governing mechanism is critically compared with existing theoretical and empirical frameworks. The results are consistent with particle packing theory as established by Wong et al. [36], which identifies particle distribution as a key factor controlling density and strength in cementitious systems. A significant relationship is also observed with biomass-based studies, with Chandrasekaran et al. [39] reporting an optimum

substitution level of approximately 10% before dilution effects become dominant. This recurring behavior suggests that the non-linear response observed in cement substitution systems is a systematic phenomenon and can be explained by the interaction between densification and reduction in active binder content.

Despite the similarities, significant differences are observed when compared with studies reporting chemical contributions from $CaCO_3$-based materials. Liu et al. [40] stated that fine $CaCO_3$ particles could modify hydration kinetics through nucleation effects, while Turcry et al. [41] reported alterations in hydration pathways due to the presence of limestone filler. Acarturk et al. [32] also observed that algal biomass could delay hydration and influence strength development. The correlation in hydration delay suggests that bio-based materials tend to influence early hydration behavior. Compared to reports on chemical interactions or phase formation, no evidence of new hydration phases was detected in this study, showing that the influence of MAD-BMF was primarily associated with physical modifications to the system, rather than chemical reactivity. These results suggest that the behavior of $CaCO_3$-based materials, particularly in bio-derived form, is context-dependent and strongly influenced by material characteristics and system conditions.

The distinction becomes more pronounced when compared with reactive systems such as LC3, according to Scrivener et al. [31]. In reactive systems, performance enhancement is attributed to pozzolanic reactions and the formation of additional hydration products that refine the microstructure. The improvements observed in this study are achieved without chemical reactivity, relying on particle-level optimization. This shows that a physically driven method can provide a more predictable strategy for designing sustainable cementitious materials.

In line with the analysis, this study supports the existing theoretical and empirical results, advancing current understanding by showing that the balance between particle packing and cement dilution serves as the primary controlling mechanism in inert filler systems. The mechanistic understanding provides a clear basis for defining performance limits and designing optimal substitution levels in a rational and systematic manner.

5. CONCLUSIONS

In conclusion, this study shows that MAD-BMF functions as a $CaCO_3$-based inert filler governed primarily by physical mechanisms. Microstructural and chemical analyses confirm the absence of new hydration phases and show a calcium-rich composition with a denser matrix structure. Compressive strength shows a non-linear response, with an optimum at 10% substitution. At low levels, strength increases due to improved particle packing and reduced porosity. Meanwhile, at higher levels, strength decreases due to cement dilution and reduced hydration product formation. Statistical analysis confirms that the behavior is consistent across curing ages. These results establish a clear mechanism based on the balance between particle packing and cement dilution. MAD-BMF provides a predictable method for reducing cement content through controlled physical effects, supporting the development of sustainable cementitious materials. Future studies should quantify PSD and SSA to establish predictive packing models for marine algae-derived fillers.

Funding

The authors received funding for this study and publication from Nusa Cendana University.

Acknowledgements

The authors are grateful for the institutional and laboratory support provided by the Civil Engineering Study Program, Faculty of Science and Engineering, including the Bioscience Laboratory and the Concrete Laboratory, Nusa Cendana University.

REFERENCES

[1] Volaity, S.S., Aylas-Paredes, B.K., Han, T., Huang, J., et al. (2025). Towards decarbonization of cement industry: A critical review of electrification technologies for sustainable cement production. Materials Sustainability, 3(23): 1-26. https://doi.org/10.1038/s44296-025-00068-6

[2] Ige, O.E., Kabeya, M. (2025). Decarbonizing the cement industry: Technological, economic, and policy barriers to CO2 mitigation adoption. Clean Technologies, 7(4): 85. https://doi.org/10.3390/cleantechnol7040085

[3] Mosly, I. (2025). Carbon footprint of global construction industries: A cross-country analysis of emissions, drivers, and the construction carbon sustainability index (1990–2023). Sustainability, 17(20): 9274. https://doi.org/10.3390/su17209274

[4] Cheng, D., Reiner, D.M., Yang, F., Cui, C., et al. (2023). Projecting future carbon emissions from cement production in developing countries. Nature Communications, 14(1): 8213. https://doi.org/10.1038/s41467-023-43660-x

[5] Zhao, Y., Dong, X., Zhou, Z., Long, J., Lu, G., Lei, H. (2022). Investigation on roles of packing density and water film thickness in synergistic effects of slag and silica fume. Materials, 15(24): 8978. https://doi.org/10.3390/ma15248978

[6] Rossignolo, J.A., Duran, A.J.F.P., Bueno, C., Martinelli Filho, J.E., Junior, H.S., Tonin, F.G. (2022). Algae application in civil construction: A review with focus on the potential uses of the pelagic Sargassum spp. biomass. Journal of Environmental Management, 303: 114258. https://doi.org/10.1016/j.jenvman.2021.114258

[7] Majid, N.B., Ibrahim, I.S.B., Nabilah Bt Sarbini, N., Zakaria, Z.A.B., Osman, M.H.B. (2019). The chemical properties of seaweed for modify concrete. IOP Conference Series: Earth and Environmental Science, 220(1): 012026. https://doi.org/10.1088/1755-1315/220/1/012026

[8] Sarbini, N.N., Ibrahim, I.S., Ismail, M., Tajol Anuar, M.Z. (2020). The effects of seaweed powder to the properties of polymer modified concrete. IOP Conference Series: Materials Science and Engineering, 849(1): 012065. https://doi.org/10.1088/1757-899X/849/1/012065

[9] de Souza, A.M., de Carvalho, J.M.F., Salgado, I.L., Santos, C.F. R., et al. (2023). Influence of filler/cement and powder/total solids on the mixture design of self-compacting micro-concretes containing waste from the

ornamental stone industry. Construction and Building Materials, 407: 133445. https://doi.org/10.1016/j.conbuildmat.2023.133445
[10] Rimmer, M.A., Larson, S., Lapong, I., Purnomo, A.H., et al. (2021). Seaweed aquaculture in Indonesia contributes to social and economic aspects of livelihoods and community wellbeing. Sustainability, 13(19): 10946. https://doi.org/10.3390/su131910946
[11] Simatupang, N.F., Pong-masak, P.R., Ratnawati, P., Agusman, Paul, N.A., Rimmer, M.A. (2021). Growth and product quality of the seaweed Kappaphycus alvarezii from different farming locations in Indonesia. Aquaculture Reports, 20: 100685. https://doi.org/10.1016/j.aqrep.2021.100685
[12] Siddique, M.N.I., Zularisam, A.W. (2018). Application of natural seaweed modified mortar for sustainable concrete production. IOP Conference Series: Materials Science and Engineering, 342: 012008. https://doi.org/10.1088/1757-899X/342/1/012008
[13] Chahbi, M., Mortadi, A., El Moznine, R., Monkade, M., Zaim, S., Nmila, R., Rchid, H. (2024). A new approach to investigate the hydration process and the effect of algae powder on the strength properties of cement paste. Australian Journal of Mechanical Engineering, 22(1): 123-132. https://doi.org/10.1080/14484846.2022.2066855
[14] ASTM C188-95. (2017). Standard test method for density of hydraulic cement. ASTM International. https://doi.org/10.1520/C0188-95
[15] ASTM C128-22. (2025). Standard test method for relative density (specific gravity) and absorption of fine aggregate. ASTM International. https://doi.org/10.1520/C0128-22
[16] ASTM C136/C136M-19. (2025). Standard test method for sieve analysis of fine and coarse aggregates. ASTM International. https://doi.org/10.1520/C0136_C0136M-19
[17] ASTM C33/C33M-18. (2023). Standard specification for concrete aggregates. ASTM International. https://doi.org/10.1520/C0033_C0033M-18
[18] Jaja, G., Ephraim, M., Johnarry, N. (2018). New absolute volume mix design method for self-compacting concrete. International Journal of Scientific & Engineering Research, 9(1): 2005-2016.
[19] Cornelis, R., Priyosulityo, H., Satyarno, I., Rochmadi, Rustendi, I. (2022). Effect of the mortar volume ratio on the mechanical behavior of class CI fly ash-based geopolymer concrete. Civil Engineering Journal, 8(9): 1920-1935. https://doi.org/10.28991/CEJ-2022-08-09-012
[20] Kandjani, A.E., Salehpoor, P., Farzalipour Tabriz, M., Vaezi, M.R. (2012). Wall effect in 3D simulation of same sized particles packing. International Journal of Engineering Transactions B: Applications, 25(2): 137-141. https://doi.org/10.5829/idosi.ije.2012.25.02b.07
[21] De Larrard, F. (1999). Concrete Mixture Proportioning: A Scientific Approach. CRC Press.
[22] Cornelis, R., Priyosulistyo, H., Satyarno, I., Rochmadi. (2019). Workability and strength properties of class C fly ash-based geopolymer mortar. MATEC Web of Conferences, 258: 01009. https://doi.org/10.1051/matecconf/201925801009
[23] ASTM C 191-21. (2026). Standard test methods for time of setting of hydraulic cement by Vicat needle. ASTM International. https://doi.org/10.1520/C0191-21
[24] ASTM C1437-20. (2020). Standard test method for flow of hydraulic cement mortar. https://doi.org/10.1520/C1437-20
[25] ASTM C109/C109M-20. (2020). Standard test method for compressive strength of hydraulic cement mortars (Using 2-in. or [50-mm] cube specimens). ASTM International. https://doi.org/10.1520/C0109_C0109M-20
[26] Boukhatem, A., Bouarab, K., Yahia, A. (2023). Kappaphycus alvarezii seaweed as novel viscosity-modifying admixture for cement-based materials. ACI Materials Journal, 120(4): 15-28. https://doi.org/10.14359/51738805
[27] Boukkhatem, A., Bouarab, K., Yahia, A. (2022). Effect of (κ)- and (ι)-carrageenans on rheology and strength development of cement-based materials. ACI Materials Journal, 119(1): 207-219. https://doi.org/10.14359/51734196
[28] Yuan, H., Ma, C., Liu, J., Ge, Z., et al. (2024). The effects of particle packing and inter-particle force on rheological behaviors of binary cement paste. KSCE Journal of Civil Engineering, 28(5): 1947-1959. https://doi.org/10.1007/s12205-024-0125-5
[29] Ji, G., Chi, H., Sun, K., Peng, X., Cai, Y. (2024). Effect of limestone waste on the hydration and microstructural properties of cement-based materials. Construction and Building Materials, 443: 137784. https://doi.org/10.1016/j.conbuildmat.2024.137784
[30] Cao, M., Ming, X., He, K., Li, L., Shen, S. (2019). Effect of macro-, micro- and nano-calcium carbonate on properties of cementitious composites—A review. Materials, 12(5): 781. https://doi.org/10.3390/ma12050781
[31] Scrivener, K., Martirena, F., Bishnoi, S., Maity, S. (2018). Calcined clay limestone cements (LC3). Cement and Concrete Research, 114: 49-56. https://doi.org/10.1016/j.cemconres.2017.08.017
[32] Acarturk, B.C., Jungclaus, M.A., Torres, M., Lash, B., Srubar, W.V. (2024). Effect of algal biomass on the properties of calcium sulfoaluminate cement. ACS Sustainable Chemistry & Engineering, 12(23): 8690-8701. https://doi.org/10.1021/acssuschemeng.4c01007
[33] Lothenbach, B., Scrivener, K., Hooton, R.D. (2011). Supplementary cementitious materials. Cement and Concrete Research, 41(12): 1244-1256. https://doi.org/10.1016/j.cemconres.2010.12.001
[34] Berodier, E., Scrivener, K. (2014). Understanding the filler effect on the nucleation and growth of C-S-H. Journal of the American Ceramic Society, 97(12): 3764-3773. https://doi.org/10.1111/jace.13177
[35] Ghasemi, Y., Emborg, M., Cwirzen, A. (2019). Effect of water film thickness on the flow in conventional mortars and concrete. Materials and Structures, 52(3): 62. https://doi.org/10.1617/s11527-019-1362-9
[36] Wong, H.H.C., Kwan, A.K.H. (2008). Packing density of cementitious materials: Part 1—measurement using a wet packing method. Materials and Structures, 41(4): 689-701. https://doi.org/10.1617/s11527-007-9274-5
[37] Fathy, A., Wagih, A., Abd El-Hamid, M., Hassan, A.A. (2014). Effect of mechanical milling on the morphology and structural evaluation of Al-Al2O3 nanocomposite powders. International Journal of Engineering, 27(4): 625-632.

https://doi.org/10.5829/idosi.ije.2014.27.04a.14
[38] Juenger, M.C.G., Snellings, R., Bernal, S.A. (2019). Supplementary cementitious materials: new sources, characterization, and performance insights. Cement and Concrete Research, 122: 257-273. https://doi.org/10.1016/j.cemconres.2019.05.008
[39] Chandrasekaran, C., Krishnamoorthy, S., Ramachandra Murthy, A., Ramesh Kumar, V., Iyer, N.R. (2018). Marine algae for cement mortar strengthening. Journal of Civil Engineering Research, 4(2A): 23-25. https://doi.org/10.5923/c.jce.201401.05
[40] Liu, S., Xiong, G., Zhao, K., Hao, L., et al. (2024). Mechanism of organic additives-induced carbonation activators on affecting cement mortars. Cement and Concrete Composites, 154: 105744. https://doi.org/10.1016/j.cemconcomp.2024.105744
[41] Turcry, P., Loukili, A., Mounanga, P., Legrand, J. (2005). Influence of limestone filler on cement hydration and chemical shrinkage at early age. In Creep, Shrinkage and Durability of Concrete and Concrete Structures CONCREEP7, Nantes, France.